

BATCH SEQUENTIAL ESTIMATION WITH NON-UNIFORM MEASUREMENTS AND NON-STATIONARY NOISE

Todd A. Ely^{*} and Jill Seubert[†]

Sequential estimation using the traditional discrete Kalman filter typically assumes the measurement time and state update time are coincident. This is often a poor assumption in realistic measurement scenarios where the data can be received from multiple sources at differing times. This paper develops the necessary algorithm adjustments needed for the Kalman filter to readily process measurement data that arrive at varying times and with non-stationary noise. The algorithm is applied to a relevant problem of orbit determination using one-way uplink radiometric tracking of a spacecraft (in the present case a Mars orbiter).

INTRODUCTION

Sequential estimation using the traditional discrete Kalman filter typically assumes the measurement time and state estimate time are coincident. This is often a poor assumption in realistic measurement scenarios where the data can be received from multiple sources at differing times. There are two ways to accommodate this: one is to apply time updates at non-uniform times and the other is to keep the time update interval fixed and process the measurement data received at the variable times between time updates of the filter in a batch. The first approach requires process noise representations that can accommodate variable intervals. Unfortunately, for a simple discrete white noise process, this invalidates the stationarity assumption of the associated noise strength. The alternative approach using an invariant time interval for the sequential batch time update can be readily modified to accommodate stationary process noise (for both dynamic and measurement state parameters) as well non-stationary process noise. This requires a modification to the traditional stochastic system equations and the associated measurement noise strengths in the Kalman filter measurement update. This paper develops the necessary algorithm adjustments needed for the Kalman filter to readily processes measurement data with non-stationary noise processes that arrive at varying times. The algorithm is applied to a relevant problem of orbit determination using one-way uplink radiometric tracking of a spacecraft (in the present case a Mars orbiter).

A GENERALIZED BATCH SEQUENTIAL FILTER

A formal representation of what we will consider is illustrated in the time line shown in Figure 1 with time flowing to the right. The timeline shown at the top illustrates a uniform cadence of filter updates, while the timeline at the bottom shows measurements arriving at non-uniform times that are different than the filter update times. The states $\mathbf{x}_k \triangleq \mathbf{x}(t_k)$, $\mathbf{x}_j \triangleq \mathbf{x}(t_j)$, $\mathbf{x}_{k+1} \triangleq \mathbf{x}(t_{k+1})$ are of interest, and the state estimate $\hat{\mathbf{x}}(t_k) \triangleq E[\mathbf{x}_k | \{\mathbf{z}_j\}]$, to be determined, is conditioned on the batch of measurements $\{\mathbf{z}_j\}$ that occur in the time interval $t_k \leq t_j < t_{k+1}$. The appearance of measurements within a batch interval is nonstandard, as the

^{*} Principal Investigator, Deep Space Atomic Clock Technology Demonstration Mission, Jet Propulsion Laboratory, California Institute of Technology, MS 301-121, 4800 Oak Grove Drive, Pasadena, CA, 91109-8099; Todd.A.Ely@jpl.nasa.gov, 818-393-1744.

[†] Deputy Principal Investigator, Deep Space Atomic Clock Technology Demonstration Mission, Jet Propulsion Laboratory, California Institute of Technology, MS 301-121, 4800 Oak Grove Drive, Pasadena, CA, 91109-8099

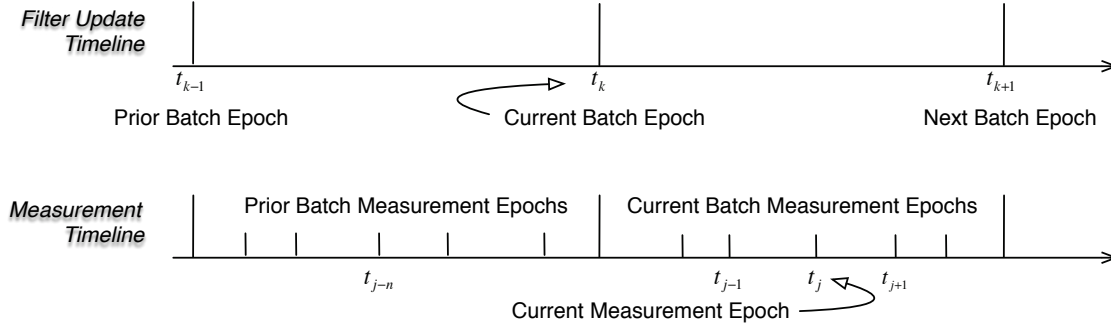


Figure 1: Batch sequential epoch timeline

traditional discrete Kalman algorithm formulation locks the state and measurement epochs to the same times and intervals; here this would be from t_k to t_{k+1} . Having measurements occurring in the interval between these two epochs acknowledges that real systems that are neither instantaneous nor uniform in time will have measurements that occur on boundaries that are not coincident with either t_k to t_{k+1} . The result is a sequence of measurements that are sensitive to a state at a defined reference epoch, typically at some time in the past. Here this is t_k and is referred to as the filter reference (or batch) epoch. Furthermore, real measurements can have non-stationary stochastic error processes (such as physical oscillator effects in one-way radiometric data types) that require expansion of the filter state vector to include components of the non-stationary process. This, in effect, makes the noise state dependent and also effects the filter model.

The fundamental problem that we are considering is a continuous nonlinear dynamical system with associated measurements arriving at discrete times. This necessitates discretizing the state equations, and in applying a Kalman filter approach, requires linearization about a nominal nonlinear reference model. This is standard and will not be reviewed here (see, for example, Maybeck [1] or Gibbs [2]). Note that the states $\mathbf{x}(\cdot)$ and associated measurements $\mathbf{y}(\cdot)$ represent *linear deviations* from their nonlinear reference values that are derived from a known (nominal) model. The true linearized deviations conform to the following model

$$\begin{aligned} \mathbf{x}_{k+1} &= \mathbf{\Phi}_{k+1,k} \mathbf{x}_k + \mathbf{w}_{k+1,k} \\ \mathbf{z}_j &= \mathbf{H}_j \mathbf{x}_j + \mathbf{v}_j \end{aligned} \quad (1)$$

where $\mathbf{\Phi}_{k+1,k}$ is the state transition matrix from time t_k to t_{k+1} . The noise processes $\mathbf{w}_{k+1,k}$ are zero-mean random variables with independent increments and strength $E\{\mathbf{w}_{k+1,k} \mathbf{w}_{k+1,k}^T\} = \mathbf{Q}_{k+1,k}$ that could depend (but not necessarily) on the selected batch time interval (t_k, t_{k+1}) . The measurement \mathbf{z}_j depends on the value of the state \mathbf{x}_j at time t_j , and \mathbf{v}_j is a zero-mean noise process with strength $E\{\mathbf{v}_j \mathbf{v}_j^T\} = \mathbf{R}_j$ and are uncorrelated in time $E\{\mathbf{v}_j \mathbf{v}_i^T\} = \mathbf{0}, i \neq j$. Furthermore, the process noise and measurement noise processes are uncorrelated $E\{\mathbf{v}_j \mathbf{w}_{k+1,k}^T\} = \mathbf{0}$ within the current batch interval. More details on the specific structure of the noise processes \mathbf{v}_j and $\mathbf{w}_{k+1,k}$ will be discussed in later examples.

Since our goal is to develop an estimator for $\hat{\mathbf{x}}(t_k)$, the state \mathbf{x}_j in Eq. (1) needs to be related to the state \mathbf{x}_k , which can be represented as follows

$$\mathbf{x}_j = \mathbf{\Phi}_{j,k} \mathbf{x}_k + \mathbf{w}_{j,k}. \quad (2)$$

It should be noted that that state transition matrix follows the traditional rules with $\mathbf{\Phi}_{k+1,k} = \mathbf{\Phi}_{k+1,j} \mathbf{\Phi}_{j,k}$, and the noise increment $\mathbf{w}_{j,k}$ overlaps with $\mathbf{w}_{k+1,k}$ so is not independent of $\mathbf{w}_{k+1,k}$. Substituting Eq. (2) into the measurement equation in Eq. (1) leads to the following expression

$$\mathbf{z}_j = \mathbf{H}_j \mathbf{\Phi}_{j,k} \mathbf{x}_k + \mathbf{H}_j \mathbf{w}_{j,k} + \mathbf{v}_j \triangleq \mathbf{H}_{j,k} \mathbf{x}_k + \mathbf{v}'_{j,k} \quad (3)$$

with $\mathbf{H}_{j,k} \triangleq \mathbf{H}_j \mathbf{\Phi}_{j,k}$ and a redefined measurement noise $\mathbf{v}'_{j,k} \triangleq \mathbf{H}_j \mathbf{w}_{j,k} + \mathbf{v}_j$ introduced to simplify notation. The associated redefined measurement noise weight is given by

$$\mathbf{R}'_{j,k} \triangleq E[\mathbf{v}'_{j,k} \mathbf{v}'_{j,k}^T] = \mathbf{H}_j \mathbf{Q}_{j,k} \mathbf{H}_j^T + \mathbf{R}_j \quad (4)$$

This is the true measurement model that is now functionally related to \mathbf{x}_k and is being driven by the original noise processes \mathbf{v}_j , but is also now dependent on the $\mathbf{w}_{j,k}$ portion of the process noise. We seek an estimator of the form

$$\begin{aligned}\hat{\mathbf{x}}_k^+ &= \hat{\mathbf{x}}_k^- + \mathbf{K}_j [\mathbf{z}_j - \mathbf{H}_{j,k} \hat{\mathbf{x}}_k^-] \vee \{\mathbf{z}_j | t_k \leq t_j < t_{k+1}\} \\ \hat{\mathbf{x}}_{k+1}^- &= \Phi_{k+1,k} \hat{\mathbf{x}}_k^+\end{aligned}\quad (5)$$

where the superscript notation '+' and '-' are typical, referring to the measurement update and time update, respectively. The term *batch sequential* refers to the fact that a batch of measurements $\{\mathbf{z}_j | t_k \leq t_j < t_{k+1}\}$ are processed before performing the time update from $\hat{\mathbf{x}}_k^+$ to $\hat{\mathbf{x}}_{k+1}^-$. To find this estimator we follow an approach similar to the Kalman filter derivation found in Crassidis [3]; however, with a key exception that the state estimate of interest is $\hat{\mathbf{x}}(t_k)$ is not coincident with t_j , and that we are processing a batch of measurements to achieve the state estimate $\hat{\mathbf{x}}_k^+$.

The covariances associated with the measurement \mathbf{P}_k^+ and time updates \mathbf{P}_k^- are defined as

$$\mathbf{P}_k^+ \triangleq E[\tilde{\mathbf{x}}_k^+ (\tilde{\mathbf{x}}_k^+)^T] \triangleq E[(\hat{\mathbf{x}}_k^+ - \mathbf{x}_k)(\hat{\mathbf{x}}_k^+ - \mathbf{x}_k)^T] \quad (6)$$

$$\mathbf{P}_k^- \triangleq E[\tilde{\mathbf{x}}_k^- (\tilde{\mathbf{x}}_k^-)^T] \triangleq E[(\hat{\mathbf{x}}_k^- - \mathbf{x}_k)(\hat{\mathbf{x}}_k^- - \mathbf{x}_k)^T] \quad (7)$$

Using the form of the desired estimator in Eq. (5) and the true model \mathbf{z}_j in Eq. (3), an expression for \mathbf{P}_k^+ can be developed

$$\begin{aligned}\mathbf{P}_k^+ &\triangleq E \left[(\mathbf{I} - \mathbf{K}_j \mathbf{H}_{j,k}) \tilde{\mathbf{x}}_k^- (\tilde{\mathbf{x}}_k^-)^T (\mathbf{I} - \mathbf{K}_j \mathbf{H}_{j,k})^T \right] + E[\mathbf{K}_j \mathbf{v}'_{j,k} \mathbf{v}'_{j,k}{}^T \mathbf{K}_j^T] + \\ &E \left[(\mathbf{I} - \mathbf{K}_j \mathbf{H}_{j,k}) \tilde{\mathbf{x}}_k^- \mathbf{v}'_{j,k}{}^T \mathbf{K}_j^T \right] + E \left[\mathbf{K}_j \mathbf{v}'_{j,k} (\tilde{\mathbf{x}}_k^-)^T (\mathbf{I} - \mathbf{K}_j \mathbf{H}_{j,k})^T \right]\end{aligned}\quad (8)$$

where, again, this is processed for all measurements in the batch $\{\mathbf{z}_j | t_k \leq t_j < t_{k+1}\}$ prior to propagating to the next time. In the typical Kalman filter derivation, the last two expectation terms in Eq. (8) are zero; however, in the current case we will consider the possibility of correlations between the redefined measurement noise $\mathbf{v}'_{j,k}$ and the filter state's process noise $\mathbf{w}_{k,k-1}$ from the prior batch. A significant measurement type used in the orbit determination applications is Doppler, which is formed via differencing two total count phase values. Because it is a construction of two measurements taken at different times, it is possible that the computed Doppler will be sensitive to both the state \mathbf{x}_k and, possibly, the state \mathbf{x}_{k-1} that occurred at an early batch boundary. In light of the dependence of $\mathbf{v}'_{j,k}$ on the process noise and the observation that the measurements could be sensitive to \mathbf{x}_{k-1} , we define the following correlation matrix $\mathbf{S}_{j,k-1} \triangleq E[\mathbf{w}_{k,k-1} \mathbf{v}'_{j,k}{}^T]$. Again, following a development similar to that found in Crassdis [3] or Lewis [4], further processing of Eq. (8) yields the following result for the covariance measurement update

$$\begin{aligned}\mathbf{P}_k^+ &= (\mathbf{I} - \mathbf{K}_j \mathbf{H}_{j,k}) \mathbf{P}_k^- (\mathbf{I} - \mathbf{K}_j \mathbf{H}_{j,k})^T + \mathbf{K}_j \mathbf{R}'_{j,k} \mathbf{K}_j^T - \\ &(\mathbf{I} - \mathbf{K}_j \mathbf{H}_{j,k}) \mathbf{S}_{j,k-1} \mathbf{K}_j^T - \mathbf{K}_j \mathbf{S}_{j,k-1}^T (\mathbf{I} - \mathbf{K}_j \mathbf{H}_{j,k})^T.\end{aligned}\quad (9)$$

The first two terms in Eq. (9) represent the typical Kalman filter measurement update result (albeit, with redefined measurement noise strength), and the second two terms are due to the potential correlation between measurement noise and prior process noise. The time update for the covariance is standard and takes the form

$$\mathbf{P}_{k+1}^- = \Phi_{k+1,k} \mathbf{P}_k^+ \Phi_{k+1,k}^T + \mathbf{Q}_{k+1,k}. \quad (10)$$

To find the gain \mathbf{K}_j we need to minimize mean squared error that is equivalent to minimizing the trace of \mathbf{P}_{k-1}^+ [3]. That is, solve

$$\min J(\mathbf{K}_j) = \min \text{Tr}(\mathbf{P}_k^+) \rightarrow \frac{\partial \text{Tr}(\mathbf{P}_k^+)}{\partial \mathbf{K}_j} = 0.$$

Doing so leads to the following result for the gain

$$\mathbf{K}_j = (\mathbf{P}_k^- \mathbf{H}_{j,k}^T + \mathbf{S}_{j,k-1}) [\mathbf{H}_{j,k} \mathbf{P}_k^- \mathbf{H}_{j,k}^T + \mathbf{R}'_{j,k} + \mathbf{H}_{j,k} \mathbf{S}_{j,k-1} + \mathbf{S}_{j,k-1}^T \mathbf{H}_{j,k}^T]^{-1} \quad (11)$$

It is possible to manipulate Eq. (9) to produce a more compact result; however, we prefer the current expression as it yields a more stable numerical implementation when taking advantage of the symmetries in the equation.

The results in Eqs. (5), (9), and (11) represent a general form for processing system measurements arriving at, potentially, *non-uniform* times, processed in a *batch* over a selected time interval, and then propagating to the next batch epoch to start the process over again; hence, *sequential* in form. It is noteworthy that with this batch sequential formulation, the measurement update must rescale the measurement noise with a portion of the state process noise in order to yield an optimal estimate. Also note that no assumption about stationarity of the noise processes has been made at this time. To motivate the preceding results, several practical problems of interest for deep space orbit determination (OD) will be explored; in particular, one-way uplink radiometric tracking where the effects of onboard clock errors, charged particle delays, and other measurement errors can be significant. These examples will explore the relative importance of the preceding development as applied first to a simple clock model and then to the OD of a Mars orbiting spacecraft.

TWO-DIMENSIONAL STOCHASTIC CLOCK AND FILTER MODEL

A continuous dynamic state model for a clock has been developed by Zucca [5] that includes the effects of deterministic bias, rate, and acceleration effects and three independent random walk (Brownian motion) stochastic processes. Davis [6] extends this to include an approximation of flicker frequency noise via the combination of several first-order Gauss Markov stochastic processes. Our purpose here is to illustrate a simple clock model's role in processing typical radiometric measurements, range and Doppler, using the preceding generalized batch sequential filter algorithm.

A clock is defined by counting the cycles of a continuously running oscillator (i.e. frequency reference or reference for short) whose ideal period can be related to the definition of the second; hence, the combination of the oscillator and the clock make an intimate pair. Clock error (or phase) $x(t)$ is defined as the deviation in time of an imperfect clock from that of an idealized perfect clock. The phase (in cycles or turns) of a *perfect* clock is given by

$$\phi(t) = f_o t + \phi_o = f_o \left(t + \frac{\phi_o}{f_o} \right) \quad (12)$$

where f_o is the nominal output frequency (in Hz), t is the time (in seconds) past some defined epoch, and ϕ_o is the initial phase at this epoch. For any real, imperfect clock, the phase is given by

$$\phi(t) = f_o(t + x(t)) \quad (13)$$

where $f_o x(t) - \phi_o$ is the measure of how the phase differs from a perfect clock. Thus, a perfect clock is just a special case of an imperfect clock where $x(t) = \phi_o / f_o = \text{constant}$. Note that the time deviation quantity $x(t)$ contains the clock bias, rate (frequency bias), and acceleration (frequency drift or aging) components as well as the stochastic processes that cause the clock to deviate from an ideal time. This representation can be utilized to form a clock that measures time with a model of the form

$$C(t) = t + x(t) \quad (14)$$

where the clock $C(t)$ is a realization of the time t but is in error by $x(t)$.

With these definitions in mind, consider a simplified continuous two-state model for a clock error process being driven by two independent stochastic processes: a random walk in phase (or white frequency noise), and a random walk in frequency. The states consist of the clock's phase error x and rate error y with the associated state vector defined as $\mathbf{x} \triangleq [x, y]^T$. The process of discretizing the continuous model correlates the resultant discrete driving noise processes [5]. The discrete dynamic model for the clock error that maps the state components from the batch epoch t_k to the measurement epoch t_j can be represented in their scalar forms as

$$\begin{aligned} x_j &= x_k + \Delta t_{j,k} y_k + w_{j,k}^1 \\ y_j &= y_k + w_{j,k}^2 \end{aligned} \quad (15)$$

where the compact notation $x_* \triangleq x(t_*)$ and $y_* \triangleq y(t_*)$ is utilized, and $\Delta t_{j,k} \triangleq t_j - t_k$, $t_j \in (t_k, t_{k+1})$. As before, we will assume that measurements arrive after the filter's batch epoch, $t_j > t_k$. The state transition matrix mapping from t_k to t_j is defined to be

$$\Phi_{j,k} \triangleq \begin{bmatrix} 1 & \Delta t_{j,k} \\ 0 & 1 \end{bmatrix} \quad (16)$$

As shown in Ref. [5], the stochastic processes $[w_{j,k}^1, w_{j,k}^2]^T$ are Gaussian variables increments that are zero mean with correlated strength

$$\mathbf{Q}_{j,k} \triangleq E \begin{bmatrix} (w_{j,k}^1)^2 & w_{j,k}^1 w_{j,k}^2 \\ w_{j,k}^2 w_{j,k}^1 & (w_{j,k}^2)^2 \end{bmatrix} \triangleq \begin{bmatrix} q_{j,k}^{11} & q_{j,k}^{12} \\ q_{j,k}^{21} & q_{j,k}^{22} \end{bmatrix} = \begin{bmatrix} \sigma_1^2 \Delta t_{j,k} + \frac{1}{3} \sigma_2^2 \Delta t_{j,k}^3 & \frac{1}{2} \sigma_2^2 \Delta t_{j,k}^2 \\ \frac{1}{2} \sigma_2^2 \Delta t_{j,k}^2 & \sigma_2^2 \Delta t_{j,k} \end{bmatrix} \quad (17)$$

It is useful to examine the $w_{j,k}^1$ process more carefully. It is comprised of two continuous Brownian motion processes $\{\beta^p(t), p \in (1,2)\}$, each with the following properties

1. $\beta^p(t)$ is a process with independent increments,
2. the increments are Gaussian random variables such that for t_1 and t_2 , any time instants in an interval of interest, the following apply

$$\begin{aligned} E[\beta^p(t_2) - \beta^p(t_1)] &= 0 \\ E[(\beta^p(t_2) - \beta^p(t_1))^2] &= \sigma_p^2 |t_2 - t_1| \end{aligned} \quad (18)$$

3. $\beta^p(t_0) = 0$ except for a set of probability zero.

These two processes are further manipulated (see Zucca [5], eq. 16) to yield the discrete random process $w_{j,k}^1$ as follows

$$w_{j,k}^1 = \delta^1(t_j, t_k) + \delta^2(t_j, t_k) = \beta^1(t_j) - \beta^1(t_k) + \int_{t_k}^{t_j} (t_j - s) d\beta^2(s). \quad (19)$$

Both the first $\delta^1(t_j, t_k)$ and the second $\delta^2(t_j, t_k)$ terms have independent increments that are, individually, Gaussian random variables. The second term $\delta^2(t_j, t_k)$ has rescaled diffusion equal to

$$E \left[(\delta^2(t_j, t_k))^2 \right] = \sigma_2^2 \int_{t_k}^{t_j} (t_j - s)^2 ds = \frac{1}{3} \sigma_2^2 \Delta t_{j,k}^3 \quad (20)$$

Because the increments are independent we have the following fact

$$E[\delta(t_j, t_k) \delta(t_{j-1}, t_k)] = E[\delta(t_j, t_{j-1}) \delta(t_{j-1}, t_k)] + E[\delta(t_{j-1}, t_k) \delta(t_{j-1}, t_k)] = \frac{1}{3} \sigma_2^2 \Delta t_{j-1,k}^3 \quad (21)$$

that we will make use of later.

The measurement vector \mathbf{z}_j for our clock will be an observation of the direct phase and differenced phases (as a proxy for Doppler) at epoch t_j and is represented as

$$\begin{bmatrix} z_j^1 \\ z_j^2 \end{bmatrix} \triangleq \begin{bmatrix} x_j + v_j^1 \\ x_j + v_j^2 - (x_{j-1} + v_{j-1}^2) \end{bmatrix} \quad (22)$$

where $[v_j^1, v_j^2]^T$ are zero mean Gaussian variables with constant noise strengths $E[v_j^1 v_j^1] \triangleq \sigma_p^2$, $E[v_j^2 v_j^2] \triangleq \sigma_d^2$, and $E[v_j^l v_k^l] = 0$ for $j \neq k$, and $l \in \{1,2\}$. These processes represent the instrument measurement errors, and not the intrinsic oscillator/clock noise (the distinction will become apparent shortly). Additionally, $[v_j^1, v_j^2]^T$ are assumed to be independent to account for differing measurement systems (i.e., Doppler derived from a phase counter versus range derived from correlating on a modulated code sequence). Following the

process used to derive Eq. (3), the measurement equations yield the following sensitivity to the state \mathbf{x}_k at the batch epoch t_k

$$\begin{bmatrix} z_j^1 \\ z_j^2 \end{bmatrix} = \begin{bmatrix} x_k + \Delta t_{j,k} y_k + w_{j,k}^1 + v_j^1 \\ \Delta t_{j,j-1} y_k + w_{j,j-1}^1 + v_j^2 - v_{j-1}^2 \end{bmatrix} \triangleq \begin{bmatrix} x_k + \Delta t_{j,k} y_k + \xi_{j,k}^1 \\ \Delta t_{j,j-1} y_k + \xi_{j,j-1}^2 \end{bmatrix} \quad (23)$$

where the process $w_{j,j-1}^1$ is the increment of the Brownian motion process in the time interval $\Delta t_{j,j-1}$ with strength $\sigma_1^2 \Delta t_{j,j-1} + \sigma_2^2 \Delta t_{j,j-1}^3 / 3$. As before, the transformation to a dependency on \mathbf{x}_k explicitly introduces process noise into the measurement equations. Note, that there is also a correlation in time introduced by the phase differencing, which violates one of the original filter assumptions. To examine the impact of this, observe for the noise process $\xi_{j,j-1}^2 \triangleq w_{j,j-1}^1 + v_j^2 - v_{j-1}^2$ that $E[\xi_{j,j-1}^2 \xi_{j-1,j-2}^2] \neq 0$. Evaluating this expectation produces

$$\begin{aligned} E[\xi_{j,j-1}^2 \xi_{j-1,j-2}^2] &= E[(w_{j,j-1}^1 + v_j^2 - v_{j-1}^2)(w_{j-1,j-2}^1 + v_{j-1}^2 - v_{j-2}^2)] \\ &= E[w_{j,j-1}^1 w_{j-1,j-2}^1] - E[(v_{j-1}^2)^2] \\ &= -\sigma_d^2 \end{aligned} \quad (24)$$

where we have made use of the independent increment property for the expectation of $w_{j,j-1}^1$ and $w_{j-1,j-2}^1$. Evaluating the rescaled measurement noise strength also yields

$$\begin{aligned} E[(\xi_{j,j-1}^2)^2] &= E[(w_{j,j-1}^1 + v_j^2 - v_{j-1}^2)(w_{j,j-1}^1 + v_j^2 - v_{j-1}^2)] \\ &= E[w_{j,j-1}^1 w_{j,j-1}^1] + E[(v_{j-1}^2)^2] + E[(v_{j-1}^2)^2] \\ &= \sigma_1^2 \Delta t_{j,j-1} + \frac{1}{3} \sigma_2^2 \Delta t_{j,j-1}^3 + 2\sigma_d^2 \\ &\triangleq 2\sigma_d^2 + q_{j,j-1}^{11} \end{aligned} \quad (25)$$

Likewise, it is determined that $E[(\xi_{j-1,j-2}^2)^2] = 2\sigma_d^2 + q_{j-1,j-2}^{11}$. We define the correlation coefficient $\rho_{j,j-1}$ using

$$\rho_{j,j-1} \triangleq \frac{E[\xi_{j,j-1}^2 \xi_{j-1,j-2}^2]}{\sqrt{E[(\xi_{j,j-1}^2)^2]} \sqrt{E[(\xi_{j-1,j-2}^2)^2]}} \quad (26)$$

which leads to

$$\rho_{j,j-1} = -\frac{\sigma_d^2}{\sqrt{(2\sigma_d^2 + q_{j,j-1}^{11})(2\sigma_d^2 + q_{j-1,j-2}^{11})}} = -\frac{1}{\sqrt{(2 + r_{j,j-1}^d)(2 + r_{j-1,j-2}^d)}} \quad (27)$$

where the relative weight of the process noise to the measurement noise is made explicit via the introduction of the ratio $r_{j,j-1}^d$, and defined as

$$r_{j,j-1}^d \triangleq \frac{q_{j,j-1}^{11}}{\sigma_d^2}. \quad (28)$$

Simplified Model to Reveal and Remove Pairwise Time Correlated Measurement Noise

To conform to the filter assumption of uncorrelated measurements in time, the measurements need to be ‘whitened’ to remove the pairwise correlation that was calculated in Eq. (27). A number of authors have developed various procedures for doing this, for instance Gibbs [2] outlines a straightforward method when the correlation between measurements can be represented using a Gauss-Markov model, $z_j^2 = \rho_{j,j-1} z_{j-1}^2 + n_j$. In the present case, the correlation is only between consecutive measurements and not more distant ones, for instance $E(z_j^2 z_{j-2}^2) = 0$. This is not consistent with the Gauss-Markov correlation model; however, as will be shown, the problem can be recast into a similar form similar. Bierman [7] provides a more applicable

‘whitening’ procedure that can be extended to the current example. To simplify the ensuing discussion, we will revert to the traditional timing relationship where the state update time and the measurement arrival time are coincident and on a uniform interval. That is, set $t_j = t_k$, $t_{j-1} = t_{k-1}$, and so forth. Compared to the previous development that led to Eqs. (5), (9), and (11), the present case shifts the indices as follows

$$\begin{aligned} j &\mapsto k \\ k &\mapsto k-1 \end{aligned} \quad (29)$$

Additionally, define

$$\Delta t \triangleq \Delta t_{k,k-1} = \Delta t_{k-1,k-2}. \quad (30)$$

The measurement equations for the phase and phase difference in Eq. (23) become

$$\begin{bmatrix} z_k^1 \\ z_k^2 \end{bmatrix} \triangleq \begin{bmatrix} 1 & \Delta t \\ 0 & \Delta t \end{bmatrix} \begin{bmatrix} x_{k-1} \\ y_{k-1} \end{bmatrix} + \begin{bmatrix} \xi_k^1 \\ \xi_k^2 \end{bmatrix} \quad (31)$$

where the measurement noise processes ξ_k^1 and ξ_k^2 are defined accordingly

$$\begin{bmatrix} \xi_k^1 \\ \xi_k^2 \end{bmatrix} \triangleq \begin{bmatrix} w_{k,k-1}^1 + v_k^1 \\ w_{k,k-1}^1 + v_k^2 - v_{k-1}^2 \end{bmatrix}. \quad (32)$$

The state vector of interest is now \mathbf{x}_{k-1} rather than \mathbf{x}_k (doing so maintains a common epoch for the state sensitivity between the two measurements). As before, the phase difference measurement noise ξ_k^2 in Eq. (31) is pairwise correlated, but the assumption of a uniform time interval simplifies the correlation to the following expression

$$\rho \triangleq \frac{E[\xi_k^2 \xi_{k-1}^2]}{\sqrt{E[(\xi_k^2)^2]} \sqrt{E[(\xi_{k-1}^2)^2]}} = -\frac{1}{2+r^d} \quad (33)$$

where $r^d \triangleq q_{k,k-1}^{11}/\sigma_d^2$ and $q_{k,k-1}^{11} \triangleq \sigma_1^2 \Delta t + \frac{1}{3} \sigma_2^2 \Delta t^3$. Note that $r^d > 0$ and $|\rho| < \frac{1}{2} \forall r^d$. The associated noise strength for ξ_k^2 is $\sigma_{\xi_2}^2 \triangleq 2\sigma_d^2 + q_{k,k-1}^{11}$. Constructing the correlated covariance matrix for the vector $\boldsymbol{\xi}_k^2 = [\xi_1^2, \xi_2^2, \dots, \xi_{k-1}^2, \xi_k^2]^T$ yields the following structure

$$\mathbf{R}_k^2 = E[\boldsymbol{\xi}_k^2 (\boldsymbol{\xi}_k^2)^T] = \sigma_{\xi_2}^2 \begin{bmatrix} 1 & \rho & & & \\ \rho & 1 & \rho & & 0 \\ & \rho & 1 & \ddots & \\ & & \ddots & \ddots & \ddots \\ 0 & & & \ddots & 1 & \rho \\ & & & & \rho & 1 \end{bmatrix}. \quad (34)$$

Bierman [7] shows that using the lower-triangular Cholesky decomposition matrix \mathbf{L}_k^2 of \mathbf{R}_k^2 , such that $\mathbf{R}_k^2 = \mathbf{L}_k^2 (\mathbf{L}_k^2)^T$, can be used to form a new noise sequence that is no longer correlated in time. The matrix \mathbf{L}_k^2 takes the form

$$\mathbf{L}_k^2 = \sigma_{\xi_2} \begin{bmatrix} \bar{\sigma}_1 & & & & & \\ \bar{\rho}_1 & \bar{\sigma}_2 & & & & 0 \\ & \bar{\rho}_2 & \bar{\sigma}_3 & & & \\ & & \ddots & \ddots & & \\ 0 & & & \ddots & \bar{\sigma}_{k-1} & \\ & & & & \bar{\rho}_{k-1} & \bar{\sigma}_k \end{bmatrix} \quad (35)$$

with $\bar{\sigma}_1 = 1$ and

$$\bar{\rho}_k = \frac{\rho}{\bar{\sigma}_k}, \quad \bar{\sigma}_{k+1} = (1 - \bar{\rho}_k^2)^{1/2}. \quad (36)$$

The new noise sequence $\boldsymbol{\zeta}_k^2 = [\zeta_1^2, \zeta_2^2, \dots, \zeta_{k-1}^2, \zeta_k^2]^T$ is defined using the inverse of the matrix square root \mathbf{L}_k^2

$$\zeta_k^2 \triangleq (\mathbf{L}_k^2)^{-1} \xi_k^2. \quad (37)$$

From this definition, Bierman [7] proves that the resultant $\{\zeta_k^2\}$ are uncorrelated with each other, $E[\zeta_i^2 \zeta_j^2] = 0$, $i \neq j$, and have strength $E[\zeta_k^2 \zeta_k^2] = \sigma_{\xi_2}^2$. He determines the recursion for ζ_k^2 to be

$$\zeta_k^2 = \frac{\xi_k^2 - \bar{\rho}_{k-1} \zeta_{k-1}^2}{\bar{\sigma}_k}, \quad k > 1. \quad (38)$$

We now make a constructive argument to recast the pairwise correlated noise ξ_k^2 as a function of the newly constructed and uncorrelated ζ_k^2 , and, in so doing, we develop a recursion for the original ξ_k^2 that allows the measurement model to be recast as one with uncorrelated noise processes. Begin by first noting that

$$\xi_k^2 = \bar{\sigma}_k \zeta_k^2 + \bar{\rho}_{k-1} \zeta_{k-1}^2 = \frac{\rho}{\bar{\rho}_k} \zeta_k^2 + \bar{\rho}_{k-1} \zeta_{k-1}^2 \quad (39)$$

and

$$\bar{\rho}_k = \frac{\rho}{(1 - \bar{\rho}_{k-1}^2)^{1/2}}, \quad k > 1. \quad (40)$$

with $\bar{\rho}_1 = \rho$. Examination of the recursion for $\bar{\rho}_k$ in Eq. (40) reveals that a steady state value $\bar{\rho}_s$ will be reached as $k \rightarrow \infty$, solving produces

$$\bar{\rho}_s = \pm \sqrt{\frac{1}{2} \pm \frac{1}{2} \sqrt{1 - 4\rho^2}} \quad (41)$$

where, using $|\rho| < \frac{1}{2}$, we note that $|\bar{\rho}_s| < \sqrt{\frac{1}{2}}$. Manipulating Eq. (39) yields the following intermediate representation of a linear difference equation for ξ_k^2

$$\xi_k^2 = \frac{\bar{\rho}_{k-1}^2}{\rho} \xi_{k-1}^2 + \frac{\rho}{\bar{\rho}_k} \zeta_k^2 - \frac{\bar{\rho}_{k-1}^2}{\rho} \bar{\rho}_{k-2} \zeta_{k-2}^2 \quad (42)$$

where, noting that $\bar{\rho}_{k-1}^2 = 1 - \rho^2 / \bar{\rho}_k^2$, leads to

$$\xi_k^2 = \frac{\bar{\rho}_{k-1}^2}{\rho} \xi_{k-1}^2 + (1 - \bar{\rho}_{k-1}^2)^{1/2} \zeta_k^2 - \bar{\rho}_{k-1} \left(\frac{\bar{\rho}_{k-1}^2}{\rho^2} - 1 \right)^{1/2} \zeta_{k-2}^2. \quad (43)$$

Recall that ζ_k^2 and ζ_{k-2}^2 are uncorrelated and each have variance $\sigma_{\xi_2}^2$, thus the linear combination of ζ_k^2 and ζ_{k-2}^2 in Eq. (43) can be recast as a new white noise process η_k^2 of the form

$$\eta_k^2 \triangleq (1 - \bar{\rho}_{k-1}^2)^{1/2} \zeta_k^2 - \bar{\rho}_{k-1} \left(\frac{\bar{\rho}_{k-1}^2}{\rho^2} - 1 \right)^{1/2} \zeta_{k-2}^2 \quad (44)$$

$$\sigma_{\eta_k}^2 \triangleq E[\eta_k^2 \eta_k^2] = \sigma_{\xi_2}^2 \left(1 - 2\bar{\rho}_{k-1}^2 + \frac{\bar{\rho}_{k-1}^4}{\rho^2} \right).$$

This yields the following, final expression for ξ_k^2

$$\xi_k^2 = \frac{\bar{\rho}_{k-1}^2}{\rho} \xi_{k-1}^2 + \eta_k^2. \quad (45)$$

The model for the noise sequence ξ_k^2 can now be used to augment the state \mathbf{x}_{k-1} so that the measurement model includes only uncorrelated (in time) noise; hence, preserving the original Kalman filter assumptions. It also retains some form of noise in the measurement model. Alternate approaches shift all of the

measurement noise into the augmented state process noise (see Reference [8]); however, doing so yields an $\mathbf{R}'_{k,k-1}$ matrix that is not positive definite or eliminates $\mathbf{R}'_{k,k-1}$ altogether. While the Kalman filter recursion will advance in this situation, it can become numerically unstable. Our approach avoids this issue. Now, the relationship of the new noise process η_k^2 to the original noise processes $\{w_{k,k-1}^1, v_k^2, v_{k-1}^2\}$ can be ascertained by comparing Eq. (32) to Eq. (45) to obtain

$$\eta_k^2 = -\frac{\bar{\rho}_k^2}{\rho} \xi_{k-1}^2 + w_{k,k-1}^1 + v_k^2 - v_{k-1}^2. \quad (46)$$

This expression will be used to evaluate measurement noise correlations between components and with the process noise.

The state vector is can be extended to include ξ_{k-1}^2 , yielding $\mathbf{x}_{k-1} \triangleq [x_{k-1}, y_{k-1}, \xi_{k-1}^2]^\top$ as the new state to be estimated. Doing so transforms the measurement model in Eq. (31) to the form

$$\begin{bmatrix} z_k^1 \\ z_k^2 \end{bmatrix} \triangleq \mathbf{H}_{k,k-1} \mathbf{x}_{k-1} + \mathbf{v}'_k = \begin{bmatrix} 1 & \Delta t & 0 \\ 0 & \Delta t & \frac{\bar{\rho}_{k-1}^2}{\rho} \end{bmatrix} \begin{bmatrix} x_{k-1} \\ y_{k-1} \\ \xi_{k-1}^2 \end{bmatrix} + \begin{bmatrix} \xi_k^1 \\ \eta_k^2 \end{bmatrix} \quad (47)$$

where the measurement noise now possesses the needed relationship $E[\mathbf{v}'_k \mathbf{v}'_{k-1}^\top] = \mathbf{0}$ and has the following strength

$$\begin{aligned} \mathbf{R}'_{k,k-1} &= \begin{bmatrix} \sigma_d^2 + q_{k,k-1}^{11} & q_{k,k-1}^{11} \\ q_{k,k-1}^{11} & \sigma_{\eta_k}^2 \end{bmatrix} \\ &= \begin{bmatrix} \sigma_p^2 + \sigma_1^2 \Delta t + \frac{1}{3} \sigma_2^2 \Delta t^3 & \sigma_1^2 \Delta t + \frac{1}{3} \sigma_2^2 \Delta t^3 \\ \sigma_1^2 \Delta t + \frac{1}{3} \sigma_2^2 \Delta t^3 & \left(2\sigma_d^2 + \sigma_1^2 \Delta t + \frac{1}{3} \sigma_2^2 \Delta t^3\right) \left(1 - 2\bar{\rho}_{k-1}^2 + \frac{\bar{\rho}_{k-1}^4}{\rho^2}\right) \end{bmatrix} \end{aligned} \quad (48)$$

The state dynamics equations can be represented as

$$\begin{aligned} x_k &= x_{k-1} + \Delta t y_{k-1} + w_{k,k-1}^1 \\ y_k &= y_{k-1} + w_{k,k-1}^2 \\ \xi_k^2 &= \frac{\bar{\rho}_{k-1}^2}{\rho} \xi_{k-1}^2 + \eta_k^2 \end{aligned} \quad \rightarrow \quad \Phi_{k,k-1} \triangleq \begin{bmatrix} 1 & \Delta t & 0 \\ 0 & 1 & 0 \\ 0 & 0 & \frac{\bar{\rho}_{k-1}^2}{\rho} \end{bmatrix} \quad (49)$$

with the associated process noise vector $\mathbf{w}_{k,k-1} \triangleq [w_{k,k-1}^1, w_{k,k-1}^2, \eta_k^2]^\top$ having the strength

$$\mathbf{Q}_{k,k-1} = \begin{bmatrix} \sigma_1^2 \Delta t + \frac{1}{3} \sigma_2^2 \Delta t^3 & \frac{1}{2} \sigma_2^2 \Delta t^2 & 0 \\ \frac{1}{2} \sigma_2^2 \Delta t^2 & \sigma_2^2 \Delta t & 0 \\ 0 & 0 & \left(2\sigma_d^2 + \sigma_1^2 \Delta t + \frac{1}{3} \sigma_2^2 \Delta t^3\right) \left(1 - 2\bar{\rho}_{k-1}^2 + \frac{\bar{\rho}_{k-1}^4}{\rho^2}\right) \end{bmatrix} \quad (50)$$

To determine if there is any correlation between the measurements and the prior process noise the following needs to be evaluated

$$\mathbf{S}_{k,k-2} \triangleq E[\mathbf{w}_{k-1,k-2} \mathbf{v}'_k^\top] = E \begin{bmatrix} w_{k-1,k-2}^1 (w_{k,k-1}^1 + v_k^1) & w_{k-1,k-2}^1 \eta_k^2 \\ w_{k-1,k-2}^2 (w_{k,k-1}^1 + v_k^1) & w_{k-1,k-2}^2 \eta_k^2 \\ \eta_{k-1}^2 (w_{k,k-1}^1 + v_k^1) & \eta_{k-1}^2 \eta_k^2 \end{bmatrix}. \quad (51)$$

Using Eq. (46) to evaluate $E[w_{k-1,k-2}^1 \eta_k^2]$ and the other correlations in $\mathbf{S}_{k,k-2}$ yields the result that $\mathbf{S}_{k,k-2} = \mathbf{0}$.

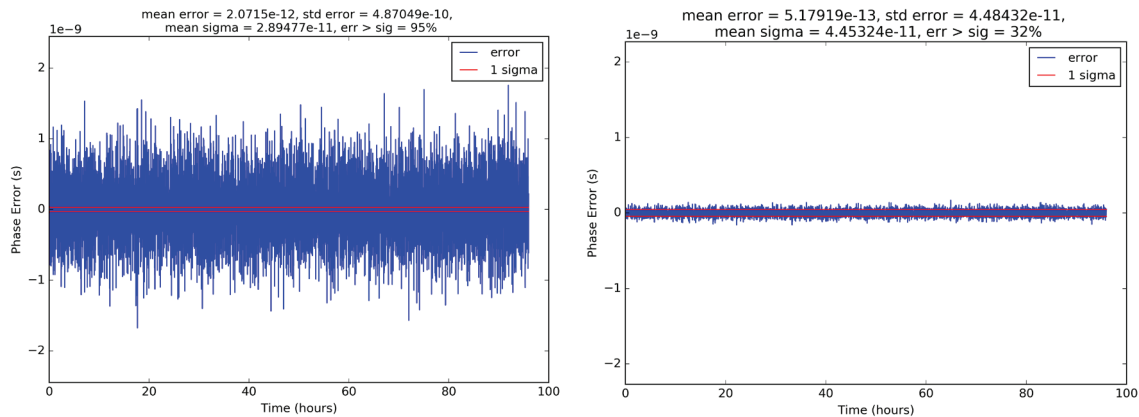


Figure 2: (left) Stochastic clock estimation without augmenting measurement noise weights with process noise nor accommodating the phase difference correlations via state augmentation. (right) Measurement weights augmented with process noise in accordance with Eq (32).

As an illustration of the preceding results, we simulate estimating the stochastic phase output of a Chip Scale Atomic Clock (CSAC), in particular a Microsemi Quantum SA.45s, with the following Allan deviation (AD) characteristics:

Table 1: CSAC SA.45s Performance Specifications

AD @ 1 second	2.5E-10
AD @ 10 seconds	8.0E-11
AD @ 100 seconds	2.5E-11
AD @ 1000 seconds	8.0E-12

This AD profile consists primarily of a random walk in phase and another in frequency. Using the values in Table 1, the associated σ_1 and σ_2 values are determined to be $8.0E-11\sqrt{\text{sec}}$ and $2.8E-14/\sqrt{\text{sec}}$. A representative measurement scenario is phase and differenced phase sampling, which represent proxies for the typical orbit determination process that utilize range and Doppler measurements. The phase and phase difference measurements are assumed independent, but with similar weights. In particular, the phase measurement has a weight of $\sigma_p = 2.0E-11 \text{ sec}$, which is consistent with phase measurement accuracy achievable from typical X-band Deep Space Network (DSN) tracking on a 60 second count. The phase difference noise weight takes the value $\sigma_p = 2.0E-11\sqrt{2} \text{ sec}$.

In the first estimation scenario of \mathbf{x}_{k-1} using measurements \mathbf{z}_k , no accommodation is made for either the process noise entering into the measurement model, as is the case in Eq (32), nor for the phase difference correlation. We call this the *naïve filter approach*. The resulting phase errors (and associated uncertainties) are shown in the plot on the left in Figure 2. The error sequence violates its 1-sigma uncertainties by a significant amount, 95% of the time, which is inconsistent with an optimally tuned filter result that should deviate approximately 32% of the time. In the second scenario, shown to the right in Figure 2 and with the same scale as the plot on the left, the measurement noise is properly deweighted with both the original measurement uncertainties and the process noise strength $q_{k,k-1}^{11}$. The most striking result is the overall phase error has been reduced by an order of magnitude as compared to the first case. Additionally, the errors have been brought into statistical agreement with their associated filter uncertainties – the errors deviate past their uncertainties 32% of the time. In the third scenario, the state vector has been expanded to include ξ_{k-1}^2 and eliminate the pairwise correlation in the differenced phase using the noise model given in Eq. (45) with the results shown in Figure 3. The left plot, again using the same scale as in Figure 2, displays the phase error results, and shows only minor improvements in overall statistics. The plot on the right exhibits the estimated (green) and truth (blue) AD values as a function of the integration time. These curves essentially overlay each other with their difference shown by the red curve. Similar AD curves (not shown) were also obtained

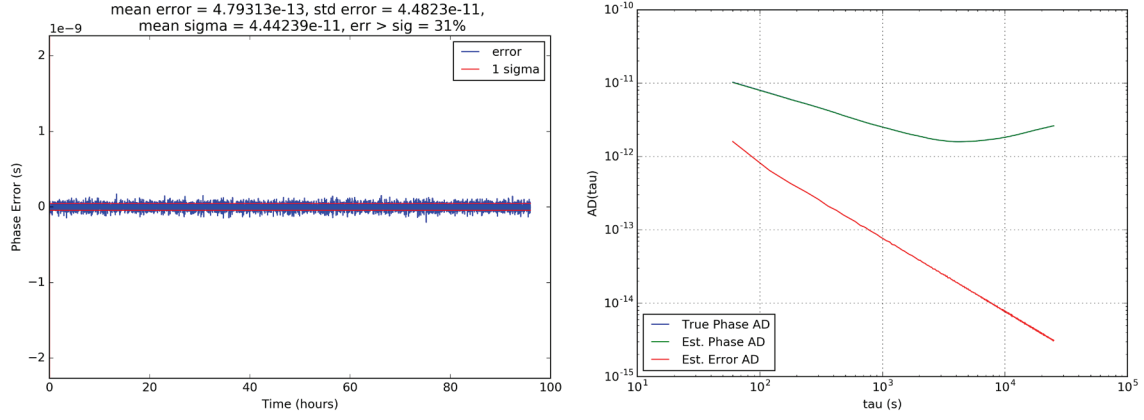


Figure 3: Stochastic clock estimation that includes both augmenting the measurement noise weights with process noise and accommodating the phase difference correlations via state augmentation.

in the previous case when only deweighting the measurements for the process noise. This indicates that the decorrelation step via state augmentation, while accurate, is not significant in this application. The critical adjustment from the naïve filter approach is the inclusion of the process noise as part of the overall measurement weight. It is noteworthy that the naïve filter approach, with no deweighting or state augmentation, yields AD values (not shown) that deviate significantly from truth by 30% on time scales out to 2000 seconds. So even though the phase errors in the left plot of Figure 2 do not display an obvious structure, there are subtle correlations that cause overall deviations in the AD on longer time scales, and shows that the naïve filter approach is suboptimal.

Phase Difference Measurement Noise and Process Noise Correlation in the 2-d Stochastic Clock

In the original scenario, where the data arrival time is more general and not tied to the batch epochs, the differenced phase data may fall across a batch boundary. In this case, $\mathbf{S}_{j,k-1}$ will have a non-zero value. To see this, assume the following time ordering

$$t_{k-1} < t_{j-1} < t_k < t_j, \quad (52)$$

and then adjust Eq. (22) to account for the placement of t_{j-1} inside of the interval (t_{k-1}, t_k) with the following result

$$\begin{bmatrix} z_j^1 \\ z_j^2 \end{bmatrix} = \begin{bmatrix} x_k + \Delta t_{j,k} y_k + w_{j,k}^1 + v_j^1 \\ \Delta t_{j,k} y_k + \Delta t_{k,j-1} y_{k-1} + w_{j,k}^1 + w_{k,j-1}^1 + v_j^2 - v_{j-1}^2 \end{bmatrix}. \quad (53)$$

The difference phase measurement z_j^2 is sensitive to the delay state y_{k-1} , which will be added to the estimated state in the current batch epoch t_k . This component y_{k-1} also participates in the state vector estimate at the prior batch epoch t_{k-1} . In order to address the measurement and phase noise correlation directly, we will forgo the decorrelation step discussed in the previous section. The measurement noise of interest \mathbf{v}'_j consists of the following components

$$\mathbf{v}'_j \triangleq \begin{bmatrix} v_j^1 \\ v_j^2 \end{bmatrix} = \begin{bmatrix} w_{j,k}^1 + v_j^1 \\ w_{j,k}^1 + w_{k,j-1}^1 + v_j^2 - v_{j-1}^2 \end{bmatrix}. \quad (54)$$

Of note is the presence of $w_{k,j-1}^1$, which is in the prior batch; hence, $\mathbf{S}_{j,k-1}$ can be evaluated with the following, non-zero result

$$\begin{aligned}
\mathbf{S}_{j,k-1} &\triangleq E[\mathbf{w}_{k,k-1}\mathbf{v}'_j{}^T] \\
&= E\begin{bmatrix} w_{k,k-1}^1(w_{j,k}^1 + v_j^1) & w_{k,k-1}^1(w_{j,k}^1 + w_{k,j-1}^1 + v_j^2 - v_{j-1}^2) \\ w_{k,k-1}^2(w_{j,k}^1 + v_j^1) & w_{k,k-1}^2(w_{j,k}^1 + w_{k,j-1}^1 + v_j^2 - v_{j-1}^2) \end{bmatrix} \\
&= E\begin{bmatrix} 0 & \sigma_1^2 \Delta t_{k,j-1} + \frac{1}{3} \sigma_2^2 \Delta t_{k,j-1}^3 \\ 0 & 0 \end{bmatrix}.
\end{aligned} \tag{55}$$

The matrix $\mathbf{S}_{j,k-1}$ will also be non-zero after decorrelation. With a careful selection of a batch epoch interval, it is possible to minimize the times when $\mathbf{S}_{j,k-1}$ is non-zero and reduce the impact of this effect on the filter solutions. Quantifying this statement and assessing the impact of a non-zero $\mathbf{S}_{j,k-1}$ for the current clock model and simulation, as well as with the Mars orbit scenario, is a topic of a future study.

APPLICATION TO MARS ORBIT DETERMINATION (OD) USING ONBOARD ONE-WAY RADIOMETRIC TRACKING

We turn our attention now to the application that initiated our study into the proper structure of a batch sequential filter. Ely and Seubert [9] detail the use of the Deep Space Atomic Clock (DSAC) for OD using onboard radiometric tracking of range and Doppler using an appropriately configured radio receiver. A summary of the radiometric model they introduced follows.

A one-way phase measurement $\Phi(t)$ is a measure of the difference of two clock signals (called the beat signal) with one being the phase of a transmitted and received radio transmission and the other generated locally within the radio receiver. All of the radiometric modeling considered in the present paper are for one-way data types that originate from a radio source (ground station, or other satellite) and are received onboard the spacecraft of interest. Two-way radiometric models are similar, but distinct. Receiver R 's phase of a beat signal $\Delta\phi(t)$ at the ideal time t is formed as the difference of the transmitted phase ϕ_T from transmitter T and the receiver's reference phase ϕ_R

$$\Delta\phi(t) = \phi_T(t - \tau) - PW(t) - \phi_R(t) = -f_T\tau - f_T[x_R(t) - x_T(t - \tau)] - PW(t) \tag{56}$$

where $PW(t)$ represents the 'phase wind-up' that results from the relative orientation changes between the receiving antenna and the transmitting antenna, f_T represents the transmission frequency (to simplify the discussion, any frequency bias that might exist between a mismatch between transmission frequency f_T and the receiver frequency f_R has been set to zero), τ is the one-way light time delay from the phase center of the transmitting antenna to the phase center of the receiving antenna and is defined as

$$\tau \triangleq t_R - t_T = t - t_T \tag{57}$$

noting that $t \triangleq t_R$. It includes the geometric path length $\Delta r(t)$ as well as delays that change the path length of the signal from other sources including ionosphere $I(t)$, solar plasma $S(t)$, troposphere $T(t)$, yielding

$$\tau(t) \cong \frac{1}{c} (\Delta r(t) - I(t) - S(t) + T(t)) \tag{58}$$

where, for phase observables, the ionosphere and solar plasma delays appear to 'shorten' the path length (in range observables these delays will 'lengthen' the path length); thus, the minus sign. For simplicity in this discussion, a Newtonian approximation for the geometric path length $\Delta r(t)$ suffices and takes the form

$$\Delta r(t) \triangleq \|\mathbf{r}_R(t) - \mathbf{r}_T(t - \tau)\| \tag{59}$$

The vectors \mathbf{r}_R and \mathbf{r}_T represent the position of receiving antenna's phase center and transmitting antenna's phase center, respectively. It should also be noted that this is a generic model and the presence of the ionosphere, solar plasma, and troposphere delays are dependent on whether the signal transits through the respective media. Their computation is also dependent on the appropriate time of transit; thus, an uplink signal from the Earth to a spacecraft receiver would evaluate the ionosphere and troposphere transit at the time $t - \tau$. For the purposes of this discussion, the functional representation of these delays on t is sufficient, where a more specific calculation must be made at the appropriate time and/or functional dependency on environment parameters will be substituted.

A receiver measuring the beat phase given in Eq. (56) will add instrument delays, noise, potentially multipath effects, and an integer ambiguity representing the number of cycles that have occurred since the signal left the satellite. These considerations result in the following one-way phase measurement model (converted into units of length)

$$\begin{aligned}\Phi(t) &\triangleq -\frac{c}{f_T}\Delta\phi(t) \\ &= \Delta r(t) + c[x_R(t) - x_T(t - \tau)] - I(t) - S(t) + T(t) + \\ &\quad PW(t) + M^\Phi(t) + b_R^\Phi(t) + b_T^\Phi + N + v(t)\end{aligned}\quad (60)$$

where $M^\Phi(t)$ is the error due to multipath effects, $b_R^\Phi(t)$ is the receiver delay, b_T^Φ is the transmitter delay (assumed static in this discussion, i.e., $\dot{b}_T^\Phi = 0$), N is the integer phase ambiguity, and $v(t)$ is the one-way measurement noise. It should also be noted that the receiver records the measurement with timetag $\mathcal{C}(t)$. With this model of one-way phase, it is now a simple matter to formulate the average one-way Doppler (in units of range rate) as the difference of adjacent phase counts separated by the Doppler count time T as follows

$$F(t) \triangleq \frac{\Phi(t) - \Phi(t - T)}{T} \quad (61)$$

Upon examination of Eq. (61), Doppler eliminates the phase ambiguity (as long as the receiver doesn't experience cycle slips or resets over the Doppler count time), and any static transmitter and receiver bias delays that would be present in the carrier phase. Only those delays that exhibit a time variation will remain in the Doppler data.

One-way ranging collected by a spacecraft receiver has a model that is very similar in form to the carrier phase model given in Eq. (61), and is formally represented using

$$R(t) = \Delta r(t) + c[x_R(t) - x_T(t - \tau)] + I(t) + S(t) + T(t) + M^R(t) + b_R^R(t) + b_T^R + \varepsilon(t) \quad (62)$$

where the differences between the range expression in Eq. (62) versus the phase in Eq. (60) include sign changes on the ionosphere and solar plasma delays, different receiver delays $b_R^R(t)$ (including temperature sensitivities), multipath, and no phase ambiguity.

Examination of the phase and range models in Eqs. (60) and (62), respectively, reveals that the receiver clock phase error $x_R(t)$ appears directly and is multiplied by the speed of light c . Hence, even the smallest clock error manifests itself in a significant way. Consider that for the typical deep space mission Doppler measurement noise at X-band is less than 0.1 mm/sec on a 60 second count time, the equivalent AD on this integration time is 3.3E-13. Additionally, as the count time increases the Doppler measurement noise strength decreases and, ideally, the impact of onboard clock errors should decrease on longer timescales. While not traditionally used in deep space applications, atomic clocks do exhibit AD profiles that are proportional to $1/\sqrt{T}$ over some extended count time. We saw earlier that a CSAC displays this characteristic; however, on short time scales, say 60 seconds, it has a short-term noise AD that is much larger than 3.3E-13. The Deep Space Atomic Clock (DSAC), currently in development by NASA/JPL, uses an Ultra Stable Oscillator (USO) for its local oscillator, typically with a short term AD near 1.E-13, and controls this to produce a stabilized frequency output with AD of better than 5.E-15 at a day (with current estimates are near 3E-15 at a day). [9] The precision of DSAC derived one-way radiometric data is near, and often better than, its two-way counterpart; hence, suitable for the most demanding deep space navigation applications. CSAC derived data is not nearly as precise but, nevertheless, may be suitable for less stringent navigation needs such as for a CubeSat mission.

We will examine the effect of the preceding estimator development as it applies to the orbit determination of a representative low-altitude Mars orbiter using one-way Doppler and range data using either CSAC or DSAC as the onboard reference. The orbiter mimics the dynamics and orbit determination procedures utilized for the Mars Reconnaissance Orbiter (MRO), but modified to account for the effects noted in the current study. Details of the high-fidelity simulation have been provided previously in Reference [10], and are not repeated here. Of relevance to the current discussion is the onboard data collection scheme, which will be described further. Because of the significant number of missions at Mars, it is reasonable to assume

that at any given time at least one DSN antenna is pointed towards the Mars. Thus, a radio signal for one-way Doppler and range data collection can be assumed to be present. Furthermore, in this study, the orbiter's receiver is configured to collect these measurements using an external reference such as DSAC, CSAC, or a USO as its reference.* In this scenario, one-way uplink-only tracking data is continuously available for processing by an onboard navigation system, except during occultations. Doppler and range X-band measurements have been generated from a high-fidelity truth trajectory and measurement models. As described in Reference [10], these truth data had numerous real world effects included both in the dynamic models (such as stochastic drag acceleration to account for atmospheric density variations, or gravitational model uncertainties) and the measurement models. The measurement models account for extended signal transit times (i.e., light time delays) and all relativistic effects including the impacts of a Mars orbiting clock. Gaussian noise degradation of the measurements is performed at the traditionally utilized 0.1 mm/sec (X-band). The stochastic clock behavior of the onboard frequency reference is either from CSAC or DSAC. The DSAC stochastic model is a white frequency noise sequence simulated in accordance with DSAC's current best estimate (CBE) performance of $3.e-15$ at one day. The CSAC noise model conforms to the statistics given in Table 1. Finally, range biases, Earth orientation errors, Earth/Mars ephemeris errors, troposphere and ionosphere delays and associated errors are included in the simulated truth measurements at levels consistent with observed values over the simulation epochs. The orbit determination filter is configured in a manner similar to MRO ground operations but adapted to account for processing one-way uplink radiometric data (versus the normal two-way DSN radiometric data collected back at Earth). The filter is a batch sequential linearized Kalman filter (LKF) using a UD factorization to ensure numerical stability.

In this first example, the only error sources included in the truth data are the stochastic clock phase and rate effects as modeled in Eqs. (15). The measurement data is simulated Earth to Mars orbiter Doppler (no range data) that includes all the high-fidelity effects mentioned previously. Hence, the tracking passes occur at physically realizable times and include data gaps due to occultations. The use of Doppler-only is representative of operational OD where range data is often not used. To best isolate the effect of the clock noise in this example the filter is configured to estimate for only the clock phase and rate terms. As before, a naïve filter approach is applied where the data is only deweighted for the standard measurement errors. That is, the deweighting for the clock process noise is not included. The clock reference used for this example is CSAC, as it more clearly depicts the effect of this mismodeling. The resulting clock phase estimate is shown in the left plot of Figure 5. The plot on the right shows the results of properly deweighting the measurements for the process noise as indicated in Eq. (4). Clearly, the later result is more optimal with only 20% of the error deviating from the one-sigma uncertainty bounds. The results shown in the left plot are not optimal, with the error being biased and the overall noise on the errors being larger than seen in the result to the right. This is the same observation noted previously with the discussion of Figure 2. It is noteworthy that while the more optimal result, while having reduced point-to-point noise levels, the overall uncertainty bounds are larger than the naïve filter's results on the left. The increase in the uncertainty bounds is expected because the overall measurement deweighting has increased. However, the reduction in the point-to-point variations is unexpected, and worth further study.

This same clock error sequence is now applied to a representative orbit determination simulation that includes all relevant errors. In this case, the orbit and other parameters (stochastic accelerations, media effects, Earth orientation, Earth/Mars ephemeris, etc.) are estimated along with the deterministic and stochastic clock parameters. Range data has been added to the measurement set and, again, CSAC is the reference. The resulting orbit errors (left-top), tracking passes (left-bottom), and clock phase errors (right) are shown in Figure 4. This solution has been 'tuned' via modifying the strength of the process white noise acceleration states that have been added to accommodate modeling errors from drag, solar pressure, and other error sources. The tuning process is ad hoc, but results in trajectory errors that are consistent with their associated statistics, at < 10 m, $1-\sigma$, and possess error sequences that minimize correlations in time. The process determines an acceleration noise strength that yields both orbit and clock solution errors that are consistent with their uncertainties (a smaller selected process noise would produce some form of bias error

* Currently most Mars missions use the Small Deep Space Transponder that is not capable of collecting range or Doppler. However, the Unified Space Transponder being currently developed by JPL is planned to have the ability to collect and/or generate one-way radiometric signals.

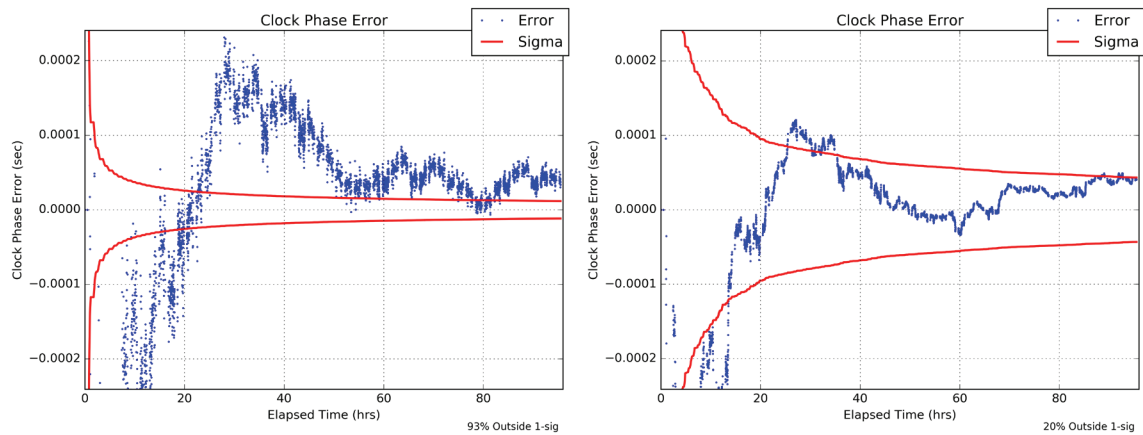


Figure 5: Stochastic clock-only estimation using Mars orbiter one-way Doppler data with CSAC as the reference. (Left) No measurement noise deweighting for stochastic clock effects, and (right) proper inclusion of these effects in the measurement deweighting.

or significant deviations away from their uncertainties). A similar study, with the local reference replaced by DSAC, yields the orbit and clock phase results shown in Figure 6 that yields orbit RSS orbit errors $< 1\text{m}$, $1\text{-}\sigma$ and improved clock solution statistics. The results are about an order of magnitude better than those with CSAC. The significant point to note is the solutions are satisfactory when using just the measurement noise deweighting as prescribed by Eq. (4). Thus, indicating, that decorrelating the Doppler measurements in time (i.e., the process that yielded Eq. (47)) is not necessary, nor is decorrelating the measurement noise from the process noise across batch boundaries (i.e., Eq. (55)) needed.

Finally, a careful examination of Eqs. (61) and (62) reveal that other measurement error processes may need to be deweighted as has been done with the oscillator noise. For example, ionosphere media delay errors are often modeled using a first-order Gauss Markov process being driven by discrete white noise that is applied on a fixed interval. A higher fidelity model could account for a variable interval, which would facilitate the application of Eq. (4). Another error source, charged particle delays from the solar plasma, are often unmodeled and accommodated via increasing the measurement noise weight using an empirical procedure. Eq. (4) could be applied with greater rigor using solar plasma noise's theoretical model, and is the subject of a future study.

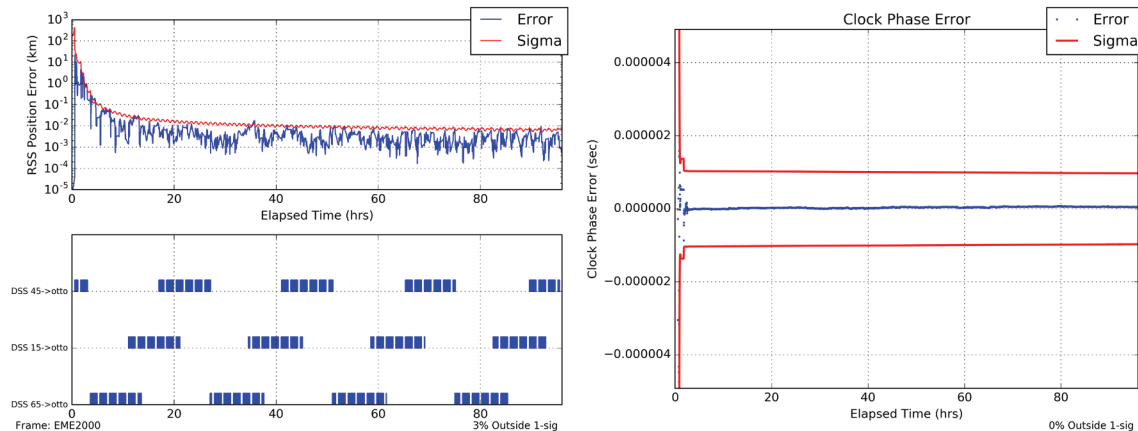


Figure 4: Orbit and clock estimation using CSAC reference with representative errors present and measurement deweighting applied. Note that the lower-left plot shows the tracking schedule between the 3 DSN stations and the Mars orbiter ('otto').

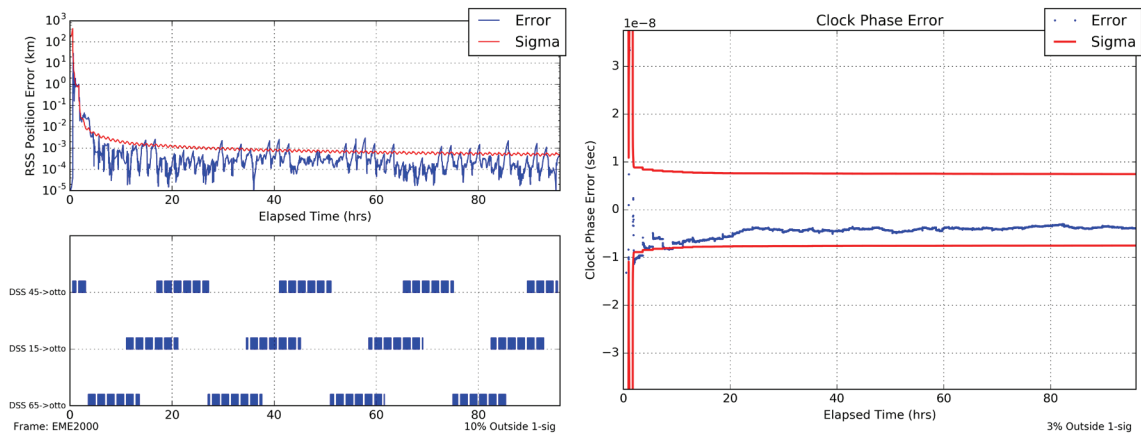


Figure 6: Orbit and clock estimation using DSAC reference with representative errors present and measurement deweighting applied. Note that the lower-left plot shows the tracking schedule between the 3 DSN stations and the Mars orbiter ('otto').

CONCLUSION

The preceding development considered the fact that real measurement systems for use in deep space orbit determination yield measurement data that is collected on non-uniform intervals. In practice, this can be accommodated in a sequential filter via processing in batches that move forward in time and measurement data that solves for a state in the recent past (aka, the filter batch epoch). Doing so requires adjustments to the standard Kalman filter equations that, effectively, deweight the measurements for the portion of process noise that might be present in the interval between the measurement time and filter batch epoch. Further adjustments might be needed to account for correlations in time that might exist with some of the measurement data. Of particular interest, is the impact of local clock stochastic noise on the processing of one-way radiometric data for deep space orbit determination. This study determined that the measurement noise deweighting procedure identified by Eq. (4) is a necessary step to achieving convergent, unbiased filter solutions. This step also proved to be sufficient for the applications studied, such that the additional steps of decorrelating the measurement data or decorrelating the measurement noise with the process noise, were not necessary. Further work is anticipated in applying these results to other significant measurement error sources, such as solar plasma noise.

ACKNOWLEDGEMENT

The research was carried out at the Jet Propulsion Laboratory, California Institute of Technology, under a contract with the National Aeronautics and Space Administration.

REFERENCES

- [1] P. S. Maybeck, *Stochastic Models, Estimation, and Control*, vol. 141–1. Orlando, Florida: Academic Press, 1979.
- [2] B. P. Gibbs, *Advanced Kalman Filtering, Least-Squares and Modeling*. Hoboken, NJ, USA: John Wiley & Sons, Inc., 2011.
- [3] J. L. Crassidis and J. L. Junkins, *Optimal Estimation of Dynamic Systems*. Boca Raton: Chapman and Hall/CRC, 2004.
- [4] F. L. Lewis, L. Xie, and D. Popa, *Optimal and Robust Estimation: With an Introduction to Stochastic Control Theory*, Second. CRC Press, 2007.
- [5] C. Zucca and P. Tavella, “The clock model and its relationship with the allan and related variances,”

IEEE Trans. Ultrason. Ferroelectr. Freq. Control, vol. 52, no. 2, pp. 289–295, 2005.

- [6] J. A. Davis, C. A. Greenhall, and P. W. Stacey, “A Kalman filter clock algorithm for use in the presence of flicker frequency modulation noise,” *Metrologia*, vol. 42, no. 1, pp. 1–10, Feb. 2005.
- [7] G. J. Bierman, *Factorization methods for discrete sequential estimation*. New York: Academic Press, 1977.
- [8] N. S. Gopaul, J. G. Wang, and B. Hu, “Discrete EKF with pairwise Time Correlated Measurement Noise for Image-Aided Inertial Integrated Navigation,” *ISPRS Ann. Photogramm. Remote Sens. Spat. Inf. Sci.*, vol. II-2, pp. 61–66, Nov. 2014.
- [9] T. A. Ely and J. Seubert, “One-Way Radiometric Navigation with the Deep Space Atomic Clock,” in *AAS/AIAA Space Flight Mechanics Meeting*, 2015.
- [10] T. A. Ely, J. Veldman, and J. Seubert, “Preliminary Investigation of Onboard Orbit Determination using Deep Space Atomic Clock Based Radio Tracking,” in *AAS/AIAA Space Flight Mechanics Meeting*, 2016.